21st Australasian Fluid Mechanics Conference
Adelaide, Australia
10-13 December 2018

Three-component Three-dimensional (3C-3D) Fluid Flow Velocimetry For Flow Turbulence Investigations

Julio Soria

Laboratory for Turbulence Research in Aerospace and Combustion
Department of Mechanical and Aerospace Engineering
Monash University
Clayton Campus
Melbourne Victoria 3800
Australia

Abstract

Advances in the last 10 years in image acquisition sensors, high quality illumination sources and cluster parallel processing have allowed us to develop and advance a number of digital techniques that enable the measurement of instantaneous three component fluid velocity vector fields in a three-dimensional volume. This paper gives a brief overview of two methods based on Incoherent Imaging, namely Tomographic PIV (TPIV) and Light-field PIV (LFPIV) and one method based on Coherent Imaging, namely Digital Holographic PIV (DHPIV). TPIV has wide acceptance in Experimental Fluid Mechanics laboratories despite its demonstrated limitations in high-fidelity turbulence measurements, whereas LFPIV and DHPIV are in many ways conceptually simpler and their limitation are current sensor technology, which with time should become less of an obstacle to their usage.

Introduction

Most flows of relevance, both industrial and environmental, are three-dimensional (3D) in nature, highly unsteady, most likely high Reynolds number and therefore, turbulent in nature containing a large range of length scales and a large dynamic range. These characteristics necessitates a measurement technique to quantify and investigate these flows that is able to measure the instantaneous three-component three-dimensional (3C-3D) velocity vector with high spatial resolution in a time-accurate manner. Today this is still an exceedingly difficult task.

In the early days film-based holographic PIV (HPIV) was one of the methods that showed promise [1, 2, 3, 4], but due to its complex implementation it did not develop into a standard laboratory tool. More recently, digital holographic recording and reconstruction [5, 6, 7, 8, 9, 10] coupled with cross-correlation PIV analysis (DHPIV) has shown promise as a 3C-3D velocity field measurement tool, but it too has its shortcoming, mainly due to the available size of sensor cells on current CCD/CMOS sensor arrays, which only permit in-line digital holographic recording. However, this limitations is becoming less severe as new CCD/CMOS sensor arrays are becoming available with micron and sub-micron sensor cells.

3D photogrammetry coupled with particle tracking has also only had limited success as a standard tool in the laboratory [11, 12, 13] — primarily due to its complex calibration requirements. However, in the last decade photogrammetry has been coupled with cross-correlation PIV analysis in a technique now referred to as Tomographic PIV (TPIV) [14, 15, 16]. This technique uses multiple cameras, typically four digital cameras and requires a calibration similar to the stereo-PIV technique. TPIV can provide 3C-3D velocity fields of unsteady and/or turbulent flows although in its standard operational form, it suffers from severe limitations in spatial resolution [17].

Apart from recording the three-dimensional position of tracer particles through the multiple view geometry of TPIV, there are other techniques that record the light-field information instead. One such technique is synthetic aperture PIV (SAPIV), which uses a large camera array, typically 8–15 cameras, to capture the light-field images of seeding particles and reconstructs 3D particle images through a synthetic aperture refocusing method [18]. SAPIV can tolerate much higher particle densities than TPIV and its dynamic velocity measurement range along the optical axis can be of the same order as the lateral directions.

A recently developed alternative, instead of using a cumbersome camera array system, uses light-field imaging to record the particle light-field image via a single plenoptic camera [19] which consists of a closely encapsulated micro-lens array (MLA) and a CCD/CMOS sensor. When coupled with cross-correlation PIV analysis we have a 3C-3D velocimetry technique, referred to as light-field PIV (LFPIV) [20, 21, 22]. LFPIV eliminates the cumbersome camera spatial calibration process, which is essential and a major source of error in TPIV. With a compact hardware setup similar as 2D-PIV, LFPIV is capable of measuring full volumetric 3C-3D velocity fields with a greatly simplified experimental procedure.

In the brief description that follows of the three experimental methods which are commonly employed in Experimental Fluid Mechanics we will distinguish them by their illumination source requirement and inherent imaging method, classifying them as either **Incoherent Imaging** or **Coherent Imaging** methods. All photogrammetry methods such as TPIV and LFPIV belong to the Incoherent Imaging family because from a fundamental point of view they do not require a coherent light source such as a laser, with other illumination such as diode illumination sufficing to illuminate the fluid volume of interest that contains the scattering tracer particles. HPIV and more specifically DHPIV belong to the Coherent Imaging family and require coherent illumination of a highly coherent laser to illuminate the fluid volume of interest that contains the scattering tracer particles.

Common to all these methods is the fundamental source of the **3C velocity signal** at a point in 3D space. This signal is provided by the tracer particle or in fact many of them which are used to seed the fluid and which must provide a high-fidelity signal of the instantaneous 3C of the velocity vector at the location where the particle is located [23, 24]. This very important aspect in fluid flow velocimetry is not within the scope of this paper nor are many other 3C-3D velocimetry methods that are use in a number of laboratories around the world (*e.g.* [25]).

The primary focus will be on the two Incoherent Imaging Methods: TPIV and LFPIV and the one Coherent Imaging Method: DHPIV.

Incoherent Imaging Methods

Incoherent imaging methods typically use multiple cameras observing the 3D domain of interest from multiple positions as shown in figure 1 or one camera as shown in figure 3 which is able to record the 3D domain of interest from multiple orientations. Although lasers are usually used in many of these applications, coherency of the light, as already mentioned, is not required and since volume illumination is used, pulsed high energy LED illumination is starting to become widely employed in these methods due to their much lower cost. A recent study has demonstrated that LED illumination outperforms laser illumination in TPIV [26].

Tomographic PIV

TPIV is a multi-stage process as shown in figure 2, consisting primarily of six stages. The first involves the digital imaging of tracer particles on multiple cameras, as is typically done in all forms of digital PIV. TPIV commonly requires the preprocess of recorded images before reconstruction. This typically involves removing the background intensity and Gaussian smoothing the images to reduce the influence of image noise, which can otherwise significantly reduce the reconstruction quality.

In order to accurately reconstruct each particle it is essential that a proper relationship is established between every point in the volume and each pixel of each camera. This process begins with the calibration of each camera, which is analogous to that performed in Stereo-PIV [27, 28]. The quality of this calibration will largely depend on the amount of distortion and warping that is created due to the facility and optics being used and can be minimised by satisfying the Scheimpflug condition and using prisms at interfaces where there is a large change in refractive index between viewing media. Calibration accuracy can be assessed by triangulating the location of each particle and mapping this location back to each camera. The disparity between the mapped location and the imaged particle location indicates the error that is present for each camera. This forms the basis of the self-calibration method [29], which uses these particle disparities to iteratively correct the calibration. After self-calibration, this disparity error can generally be reduced to ≤ 0.1 pixel, albeit at a loss of spatial location accuracy.

Tomographic reconstruction is performed using algebraic reconstruction methods that involve the discretization of the measurement volume in a uniform volumetric grid of points, often referred to as voxels. A weighting matrix is then used to represent the contribution of the intensity in each voxel to the intensity seen by each pixel of each camera. The exact formulation of this matrix varies for different methods. Nevertheless, geometrically this should represent the intersection of the cone of vision of each pixel, with the cubic voxel. Typically, this intersection is represented by the intersection of a cylinder and a sphere with cross-sectional area and volume corresponding to that of a pixel and a voxel, respectively [16]. The accuracy of this weighting matrix will depend on the accuracy of the calibration process with the discretization and weighting representation also affecting the reconstruction. The standard practice is to use voxel dimensions roughly equal to the pixel size in the measurement domain.

Reconstruction involves estimating 3D distributions of particle intensities from a limited number of 2D images and as such is a highly ill-posed problem with multiple possible solutions. Solutions therefore not only depend on the number of iterations performed, but may not converge to the true particle distributions. In practice, this is almost always the case, where the ambiguity in the reconstruction leads to the formation of both real particles and ghost particles. Reconstructed particles also tend to be slightly elongated through the light sheet thickness since cameras generally share a similar depth of field direction, the effect of which is illustrated in [16]. Ghost particles are defined as intensity peaks that do not correspond to actual measured particle locations, but rather are created by the presence of multiple particle locations that can satisfy the recorded 2D images. Fortunately, algebraic reconstruction algorithms spread intensity across these locations so that ghost particles tend to have a lower intensity than true particles [15, 16]. As the number of ghost particles increases, however, this difference in intensity is reduced. Ghost particles can act as noise in the correlation plane but as discussed in [16], these ghost particles inherit velocity from neighbouring true particles and as such can spread velocity across the volume, resulting in loss of spatial resolution.

The determination of three-component (3C) particle displacements throughout the volume requires the division of reconstructed particle intensity volume pairs into a series of 3D sub-volumes, which are then 3D cross-correlated. This process is completely identical in all respects to 2C-2D cross-correlation PIV analysis except that it has been extended from 2D to 3D. The effects of cross-correlation and peak-fitting algorithms have been extensively studied with respect to 2C-2D cross-correlation PIV, *e.g.* [30] and many others. The conclusions from this work show the existence of a systematic bias error or underestimation of velocity, a bias towards integer displacements, often referred to as peak locking, and an increasing uncertainty in regions of large velocity gradients. Each of these will also contribute a similar error to the TPIV process.

The in-depth study of the accuracy of TPIV in measurements of a high Reynolds number turbulent boundary layer (TBL) by [17] demonstrated that the uncertainty of the velocity measurements is around 0.4 px after appropriate filtering. However, the largest limitation of TPIV was found to be a spatial dynamic range (SDR) estimated at SDR ≈ 7.0 with the smallest resolvable structures being 3 times larger than the smallest expected coherent structures at the Reynolds number of the TBL under investigation. Gaussian smoothing improves the visualisation of the larger scale structures in the flow, as shown in figure 4. However, it cannot recover the true turbulent signal at large wave numbers. Limitations on image seeding density, the distribution of this seeding across the volume and reconstruction noise suggest that TPIV has a lower effective spatial resolution than either planar or Stereo-PIV. As in all optically based experiments, a compromise must be made between the desired measurement accuracy, the magnification required to achieve this, the desired measurement domain and the ultimate aim of the experimental measurements.

Light-field PIV

A significant limitation of TPIV is that it requires the use of multiple views and cameras, the arrangement of which necessitates the use of a large experimental workspace and multiple paths of optical accesses to the measurement area. This may be problematic for many space-constrained applications and internal industrial flows where it may not be possible to have multiple optical windows or to perform in situ camera calibration. Hence, a single-camera-based volumetric flow diagnostic techniques with large measurable volume and high spatial resolution are highly desirable for these space-constrained applications and in general. One such technique is the single-camera-

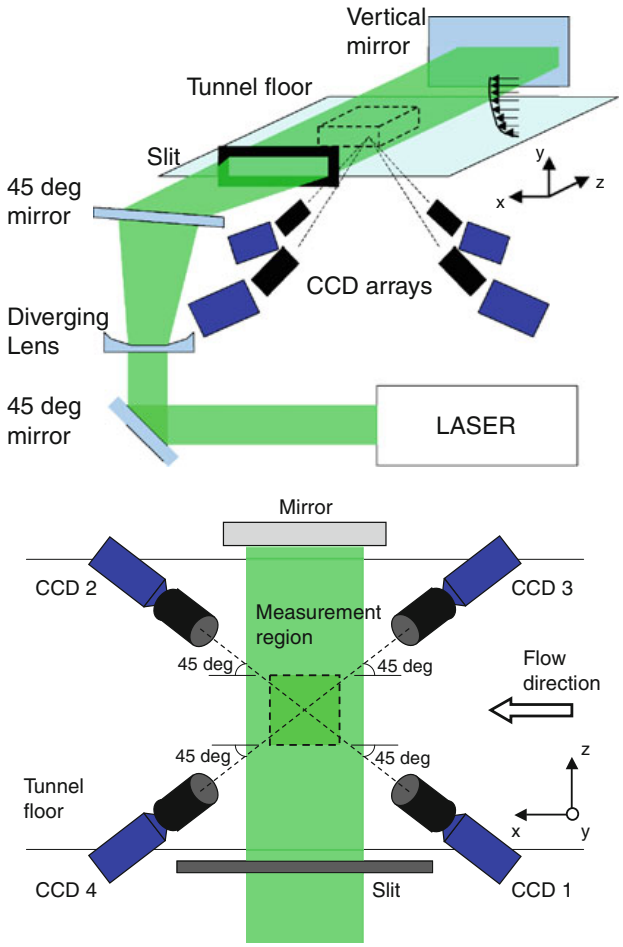

Figure 1: Typical multi-camera setup for TPIV to measure the 3C-3D velocity field of a turbulent boundary layer [17].

based light-field particle image velocimetry (LFPIV).

LFPIV relies on light-field photography to capture 3D information of tracer particles. Unlike SAPIV which employs a camera array to record the light-field of particle images, LFPIV achieves a similar functionality using a light-field camera, which combines a high-resolution microlens array (MLA) with a CCD/CMOS sensor as shown schematically in figure 5. The identification of key performance parameters in LFPIV is not straightforward. In a light-field camera the MLA is positioned one focal length away from the CCD/ CMOS sensor, which ensures the highest available angular resolution as shown in 5 (a). In a focused light-field camera as shown in 5 (b), the distance between the MLA and CCD/CMOS sensor is variable and different levels of spatial resolution, *i.e.* resolution in each refocused slice, can be achieved by sacrificing angular resolution.

For volumetric fluid velocity measurements, higher angular resolution is preferred over the in-plane spatial resolution as it leads to improved information of the particle displacement in the direction normal to the imaging plane. Hence, current LFPIV techniques all make use of light-field cameras [20, 21, 22]. The performance of LFPIV is primarily affected by the pixel–to-microlens ratio (PMR) as angular resolution is determined by the number of pixels beneath each lenslet. In addition, higher MLA resolution can tolerate higher seeding density [31]. Therefore, it is preferable for LFPIV to achieve as high a pixel resolution as possible, so as to produce high angular resolution (large PMR) as well as high spatial resolution

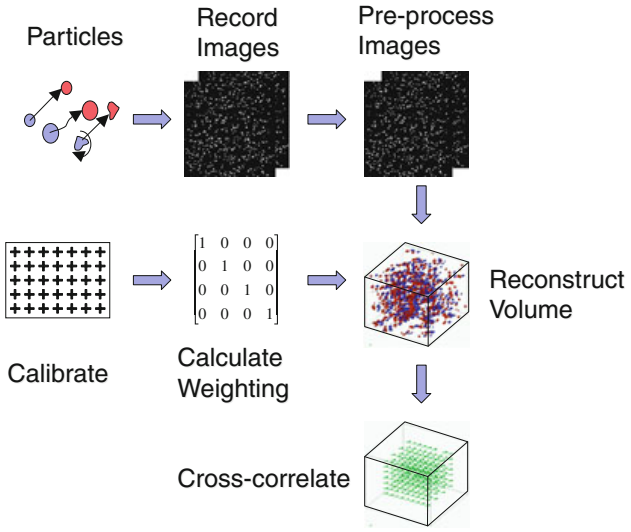

Figure 2: The different stages of TPIV processing.

(high MLA resolution). Therefore, PMR is the key factor that affects the performance of LFPIV.

A recent study by [22] has investigated this key factor and compared LFPIV to TPIV, both using synthetic computer generated data and using the experimental data from the turbulent jet experiment shown in figure 3. With respect to the latter, figure 6 shows for comparison the phase-averaged jet flow fields measured by LFPIV and TPIV. Specifically, the vorticity together with velocity vectors (colours represent the velocity component in the jet direction) are shown. Both LFPIV and TPIV capture the vortex roll-up along the jet shear layer, with the overall flow structure looking similar between the two techniques. A cross-correlation between these two measured flow fields indicates that the correlation coefficient is 0.94, suggesting a high level of agreement between the LFPIV and TPIV results.

This study [22] also demonstrated that the single-camera LFPIV can achieve an accuracy equivalent to or better than the multi-camera TPIV for the same field of view, but doing so requires a relatively high PMR and light-field camera tomo-to-camera pixel ratio (LTPR). For the same total number of pixels, the single-camera LFPIV cannot match the seeding density or spatial resolution of TPIV due to its smaller angular resolution. Nevertheless, this study points out the significant potential of this single-camera-based volumetric velocity measurement technique, owing to its greater simplicity and its ability to provide accurate 3C-3D flow measurements, particularly in applications where optical access is limited.

Coherent Imaging Method - Digital Holographic PIV

In contrast to TPIV and LFPIV, DHPIV, using coherent imaging via digital holographic recording and digital holographic reconstruction, provides the 3D intensity field of all particles in a 3D volume directly from a single sensor and without the complex optical calibration which is essential in TPIV. Two sequentially recorded 3D intensity field of all particles can subsequently be analysed using 3D cross-correlation analysis. as is done in TPIV. The basic set-up for in-line digital hologram recording shown in figure 7 is described in [7, 8, 10]. Note that the purpose of the lenses in the arranagment shown in figure 7 is to produce a collimated laser beam of sufficient diameter to illuminate the sample volume of interest and as a minimum the entire CCD/CMOS sensor.

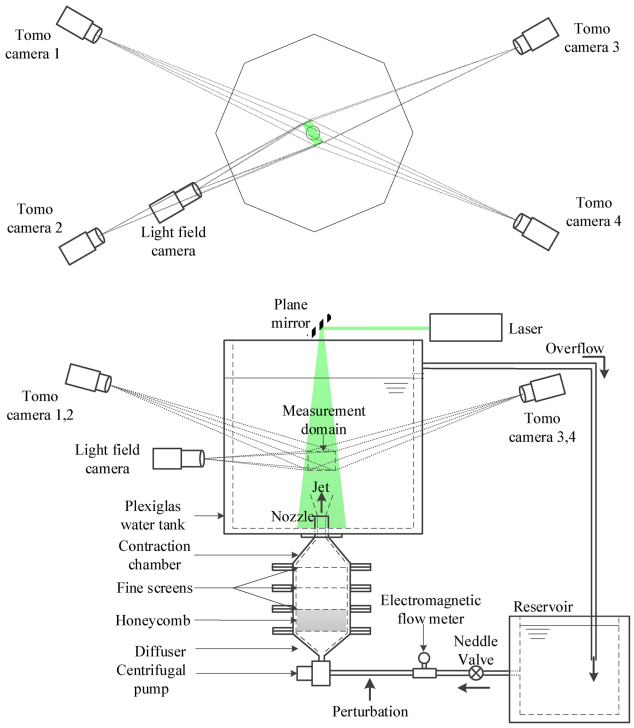

Figure 3: Typical multi-camera setup for TPIV compared to the much simpler 1 plenoptic camera LFPIV setup to measure the 3C-3D velocity field of a turbulent jet [22].

This laser beam is used to illuminate sample objects, *e.g.* micron or sub-micron particles, as shown in figure 7. The laser light scatters from these particles, while the unobstructed laser light propagates to the CCD/CMOS sensor and acts as the reference laser illumination. The scattered laser light and that of the collimated reference beam interfere on the CCD sensor to form an interference pattern, which is referred to as the digital hologram.

The process of digital hologram reconstruction is, in principle, similar to the process of reconstructing an optical hologram. The hologram intensity distribution recorded on the electronic sensor, which is identified by the Cartesian coordinate system (x, y, z = 0), is multiplied by the reference (or its conjugate) wave and the resulting wave $I_H(x,y,0)$ is numerically propagated to the virtual (or real) image plane. The complex amplitude distribution $U(x_0,y_0;z)$ in any plane, which is a distance z normal from the hologram position, *i.e.* from the electronic sensor plane, can be calculated from $I_H(x,y,0)$ using the Rayleigh–Sommerfeld diffraction formula [33],

$$U(x_0,y_0;z) = \frac{1}{\imath\lambda}\int_\Sigma I_H(x,y,0)\,\frac{\exp(\imath k r_{01})}{r_{01}}\cos(\vec{n},\vec{r_{01}})\,dxdy \tag{1}$$

where λ and $k = \frac{2\pi}{\lambda}$ is the wavelength and wavenumber respectively of the illumination used during the recording of the digital hologram. $r_{01} = \sqrt{(x-x_0)^2+(y-y_0)^2+z^2}$ is the distance from a point $(x,y,0)$ on the electronic sensor to any point (x_0,y_0,z) in the reconstructed image plane identified by the distance z from the electronic sensor with $\vec{n}$ the outward unit normal of the diffraction surface [33]. The obliquity factor $\cos(\vec{n},\vec{r_{01}})$ for most practical applications can be readily approximated by

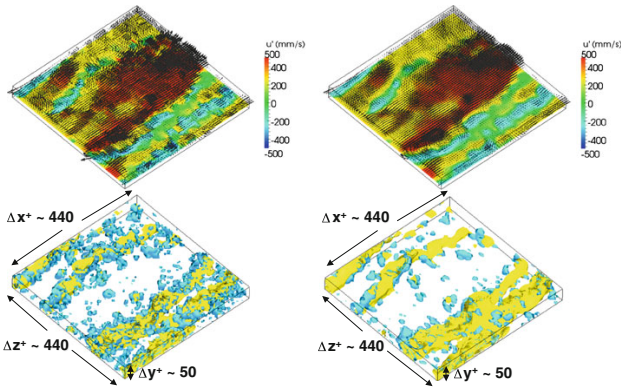

Figure 4: Instantaneous fluctuating velocity fields produced by TPIV at $Re_\theta = 7,800$. (Left) raw unfiltered velocity field and contours. (Right) $3\times3\times3$ Gaussian filtered velocity fields and contours. Mean velocity has been removed. Vectors are shown for a single plane at $y^+ = 27$. *Yellow* iso-contours represent regions of low-speed velocity, *blue* iso-contours represent vortices as identified by the discriminant [32].

$$\cos(\vec{n},\vec{r_{01}}) \approx 1 \tag{2}$$

for typical dimensions involved in digital hologram recording. This permits equation (1) to be written as the convolution integral

$$U(x_0,y_0;z) = \int_\Sigma I_H(x,y,0)\,h(x_0,y_0,z;x,y)\,dxdy \tag{3}$$

which is interpreted as the convolution between $I_H(x,y,0)$ and the diffraction kernel given by:

$$h(x_0,y_0,z;x,y) = \frac{\exp(\imath k r_{01})}{\imath\lambda r_{01}} \tag{4}$$

Defining the Fourier transforms, $\mathcal{F}[\ ]$, of $I_H(x,y,0)$ and the diffraction kernel by

$$\begin{aligned} I_H(f_x,f_y) &= \mathcal{F}[I_H(x,y,0)] \\ H(f_x,f_y;z) &= \mathcal{F}[h(x_0,y_0,z;x,y)] \end{aligned} \tag{5}$$

respectively, allows the complex amplitude distribution in the image plane to be numerically calculated in an efficient way using

$$U(x_0,y_0;z) = \mathcal{F}^{-1}[I_H(f_x,f_y)\,H(f_x,f_y;z)] \tag{6}$$

where $\mathcal{F}^{-1}$ represents the inverse Fourier transform. In practice the Fast Fourier transform is used to compute equations (5) and (6).

In digital hologram reconstruction approach using equation (6) the method developed by [34] is recursively implemented to determine the reconstructed planar image intensities of the particles in several closely spaced planes normal to the z-coordinate direction, where the spacing of these planes should correspond to the in-plane spatial resolution. The [34] technique utilizes an iterative filter that limits the twin-image effect (*i.e.* the real and virtual images), common to all in-line holograms, by averaging.

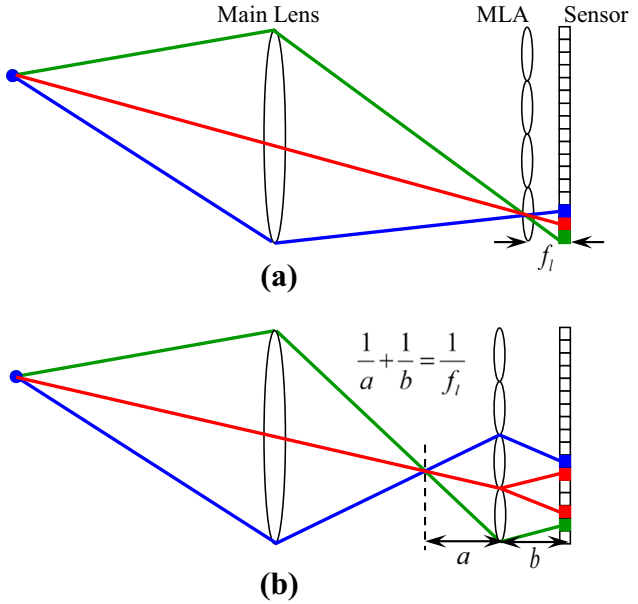

Figure 5: Schematics of light-field imaging techniques based on: (a) light- field camera and (b) focused light-field camera.

Figure 8 illustrates the results of the different stages: (a) is an example of a digitally recorded hologram while (b) shows the intensity cross-sections of a particle (indicated in (a)) as a function of reconstruction distance z_0 from the sensor. Figure 8 (c) shows the diameter variation as a function of z_0, clearly indicating that the reconstructed diameter varies by less than 3% from a value of 140μm over a domain of z_0 equal to 2.4 mm, which is clearly not physical. Figure 8 (c) also shows the standard deviation of the reconstructed image intensity, σ_i plotted as a function of the distance z_0 from the CCD sensor (Δz_0= 0.1 mm). The minimum of σ_i occurs at –88.8 mm and the droplet size at this position is 140.1 μm, which identifies the particle diameter.

The particle elongation demonstrated in Figure 8 had been previously observed by [8] among others, who found that the digital reconstruction of digital in-line holograms described above reconstructs particles of 90 μm diameter with an estimated linear in-line dimension of approximately 15.2 mm, (*i.e.* the ellipsoidal major axis of the reconstructed particle is in the z-coordinate direction) as shown in figure 9. This effect is known as the depth-of-field problem of in-line holography [8]. Possible means of overcoming the depth-of-field problem suggested by [8] include particle side scattering, off-axis holography and the tomographic approach to DHPIV proposed by [35].

The use of side scatter requires optical elements that add complexity and can possibly distort the particle images. Furthermore, this approach requires more powerful lasers than required for in-line holography, typically going from milli-Watts to 100 Watts. Off-axis holography, on the other hand, also has its limitations: the angle-dependent wavenumber of the interference pattern formed by the reference and object beams during off-axis hologram recording is $\zeta = \frac{\sin\theta}{\lambda}$. The maximum wavenumber that can be resolved by the CCD/CMOS array sensor is the inverse of twice the pixel size: $\zeta_{max} \approx \frac{1}{2\Delta}$. For typical CCD/CMOS array sensor, which have a pixel size of 6-7 μm and Nd:YAG laser illumination with a wavelength $\lambda = 532nm$, this yields a maximum angle of about $\theta_{max} \approx 2.1^0$. However, in order to separate the real and virtual images a minimum angle of $\theta_{min} = \sin^{-1}(B\lambda)$ is required (where B is the maximum spatial frequency of the image). For PIV applications, given sparse

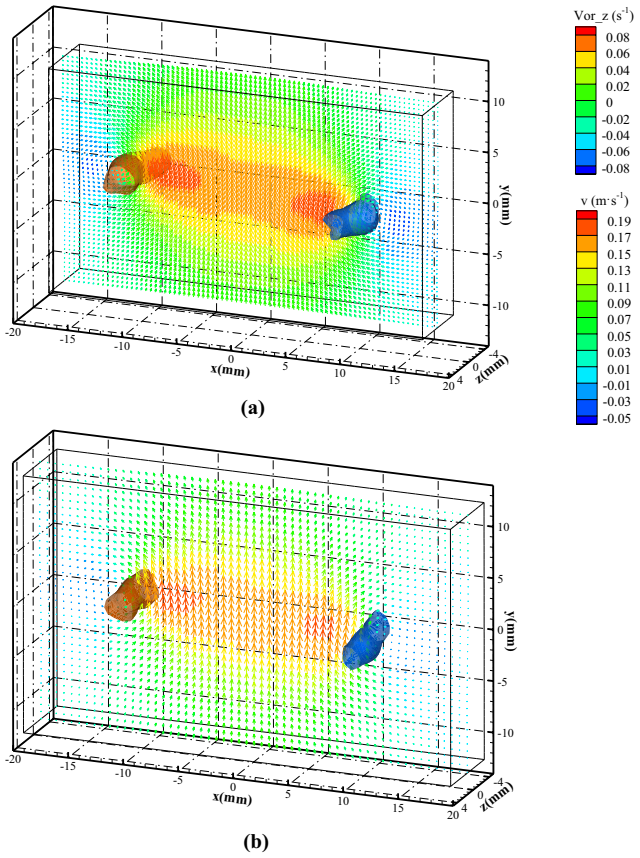

Figure 6: Phase-averaged jet flow field measured by: (a) LF-PIV and (b) Tomo-PIV of a round jet with diamter $D = 20$ mm and $Re_D = 2,000$ [22].

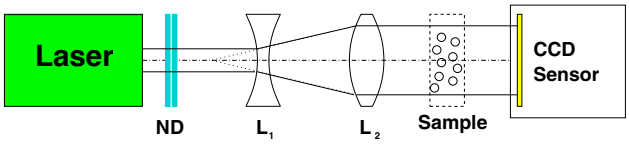

Figure 7: Typical experimental arrangement for in-line digital hologram recording (plan view), ND = neutral density filter, L_1 = diverging spherical lens, L_2 = converging lens.

seeding and large particles these competing effects can be satisfied, but only for a small object field that is located relatively far away from the CCD/CMOS array sensor. This severely limits the application of off-axis holographic recording in macro Fluid Mechanics experiments and for these flows in-line DHPIV is hologram recording method of choice. A number of recent additional approaches that overcome the depth-of-field problem of in-line holography use a magnification [36] or microscopy [37] approach to record a magnified hologram. However, this approach comes at the expense of the proportionally reduced spatial domain that can be measured.

From a fundamental point of view DHPIV is the most appealing of the three 3C-3D PIV (or particle tracking (PTV)) techniques described in this paper with the main advantage that this approach does not require any optical calibration. It simply requires a low-energy coherent laser, two lenses to enlarge the laser beam into a collimated beam that encompasses the flow domain of interest and a digital sensor with small pixels. With respect to the latter, large sensor arrays of the order of 50 MPx are becoming available with a pixels size of 5.5 μm. When cou-

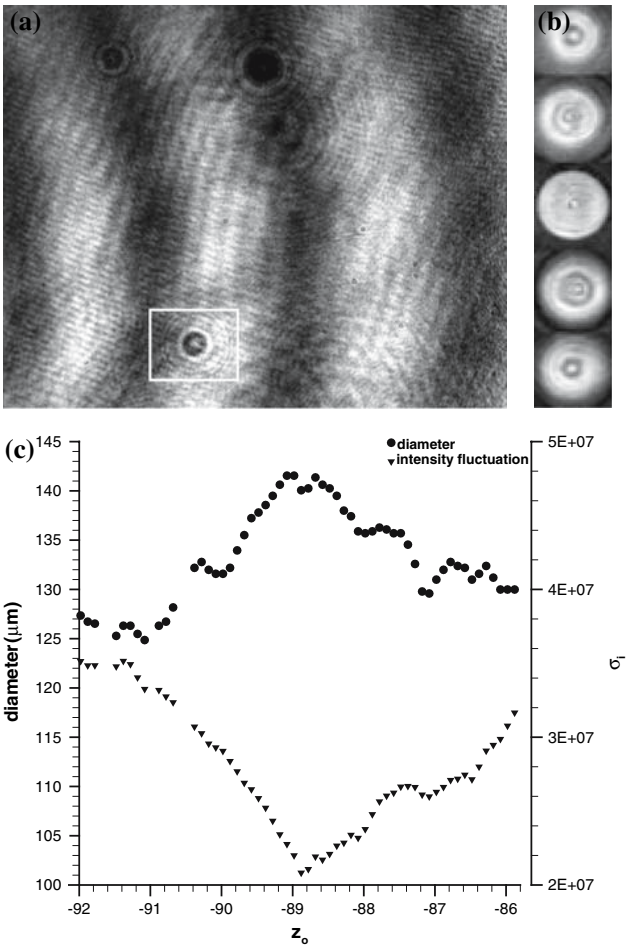

Figure 8: (a) Digital in-line hologram, (b) reconstructed particle for z_0 ranging from –85 to –93 mm, (c) particle diameter and standard deviation of the reconstructed image intensity as a function of z_o.

pled with a 10X microscope, in a micro-DHPIV arrangement [36], the effective pixel size is of the order of the typical laser illuminating wavelength, *e.g.* $\lambda = 532\ nm$, enabling the instantaneous 3C-3D fluid velocity vector field measurement in a fluid volume with a typical projected area of 5 mm x 3 mm at the spatial resolution of the wavelength of the laser. Therefore, even from the point of view of spatial resolution, DHPIV is unsurpassed by TPIV or LFPIV.

Improvements of 3C-3D Techniques via High-repetition Acquisition

Having available sensors and illumination sources that can acquire *"signals"* at high repetition rates, yielding time series of these signals where the tracer particles (*i.e.* the signals) move less than a small multiple of their size between acquisitions, enables all three techniques described in this paper to enhance their precision, reduce their uncertainty and noise and significantly increase their spatial resolution.

This has recently been demonstrated with respect to TPIV [38], but it is obvious that all 3C-3D PIV techniques would benefit from the availability of the additional time information, if available. In most liquid flows this is typically not a problem, however in gas flows the required temporal acquisition is significantly higher and the necessary CCD/CMOS array sensors and illumination sources are currently not in general available.

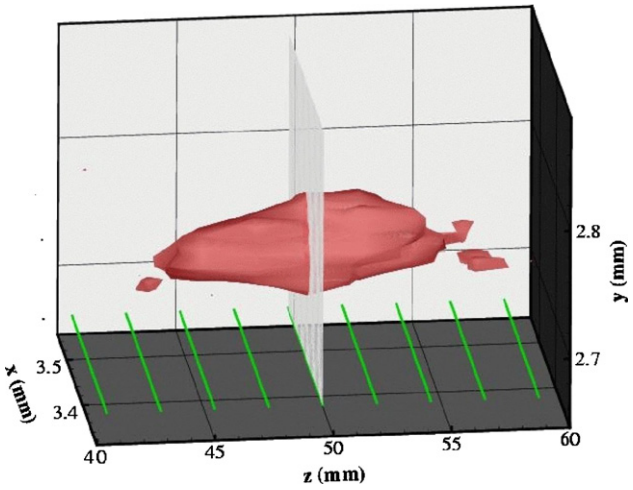

Figure 9: Digital hologram reconstruction of a 90 μm diameter particle recorded using in-line digital holography. The central plane at z = 49.7 mm is shown as a grey sheet and the green lines correspond to the locations of the other reconstruction planes [8].

But it must also be said that it is only a matter of time until the necessary CCD/CMOS array sensors and illumination sources become more generally available.

Concluding Remarks

This paper provides a brief introduction and description to two 3C-3D Incoherent Imaging based particle velocimetry techniques, namely TPIV, which is reasonably well established and LFPIV, which is promising and is expected to become more prominent as larger CCD/CMOS array sensors become available, and one Coherent Imaging based particle velocimetry technique, namely DHPIV, which is seeing a renaissance due to new CCD/CMOS array sensors.

These three techniques are currently used in Experimental Fluid Mechanics and Turbulence research as well as applied research industrial measurements. They are also topics of measurement physics research in their own right. The advantages and disadvantages of each technique, some of which are inherently fundamental to their operational principle and some which are only technological in nature have been briefly highlighted. The most appropriate technique for a particular task, as always, depends on the aims of the experiment, the measurements required to achieve those aims, their precision, uncertainty, noise level and spatial resolution sought for the environment or experimental facility, and certainly should not be guided by fashions.

Acknowledgements

This research is funded through ARC Discovery and Linkage grants supported by the Australian Government, which is gratefully acknowledged. The research also benefited from computational resources provided through the National Computational Merit Allocation Scheme, supported by the Australian Government via the computational facilities provided by the Australian National Computational Infrastructure (NCI) facility, the partner share of the NCI facility provided by Monash University through a ARC LIEF grant and the Multi-modal Australian ScienceS Imaging and Visualisation Environment (MASSIVE) at Monash University.

References

[1] DH Barnhart, RJ Adrian, and GC Papen. Phase-conjugate holographic system for high resolution particle image velocimetry. *Applied Optics*, 33(30):7159–7170, 1994.

[2] F Hussain, D D Liu, S Simmonds, and H Meng. Hpiv prospects and limitations holographic particle image velocimetry. *FED*, 148:1–11, 1993.

[3] A Lozano, J Kostas, and J Soria. Use of holography in particle image velocimetry measurements of a swirling flow. *Experiments in Fluids*, 27:251—261, 1999.

[4] K von Ellenrieder, J Kostas, and J Soria. Measurements of a wall-bounded turbulent, separated flow using HPIV. *Journal of Turbulence*, 2:1–15, 2001.

[5] S Coëtmellec, C Buraga-Lefebvre, D Lebrun, and C Özkul. Application of in-line digital holography to multiple plane velocimetry. *Measurement Science and Technology*, 12:1392–1397, 2001.

[6] S Murata and N Yasuda. Potential of digital holography in particle measurement. *Optics and Laser Technology*, 32:567–574, October 2000.

[7] G Pan and H Meng. Digital holography of particle fields: reconstruction by use of complex amplitude. *Applied Optics*, 42(5):827–833, February 2003.

[8] K von Ellenrider and J Soria Experimental measurements of particle depth of field in digital holography. In *International Workshop on Holographic metrology in Fluid Mechanics*, 2003.

[9] J Lobera, N Andrés, and M P Arroyo. Digital speckle pattern interferometry as a holographic velocimetry technique. *Measurement Science and Technology*, 15:718–724, 2004.

[10] V Palero, M P Arroyo, and J Soria. Digital holography for micro-droplet diagnostics. *Experiments in Fluids*, 43(2):185–195, August 2007.

[11] N A Malik, Th Dracos, and D A Papantoniou. Particle tracking velocimetry in three-dimensional flows. *Experiments in Fluids*, 15:279–294, 1993.

[12] NA Malik, Th Dracos, and D Papantoniou. PTV in 3-D flows; Part II : Particle Tracking. *Experiments in Fluids*, 15:279–294, 1993.

[13] Y. K. Sato, N. Kasagi, and N. Takamura. Application of the three-dimensional particle tracking velocimeter to a turbulent air ßow. In *Proceedings of third Asian Symposium on Visualization*, pages 705 – 709, 1994.

[14] M Ciofalo, M Signorin, and M Simiano. Tomographic particle-image velocimetry and thermography in Rayleigh-Bernard convection using suspended thermochromic liquid crystals and digital image processing. *Experiments in Fluids*, 34:156–172, 2003.

[15] GE Elsinga, F Scarano, B Wieneke, and BW Van Oudheusden. Tomographic particle image velocimetry. *Experiments in Fluids*, 41(6):933–947, 2006.

[16] C Atkinson and J Soria. An efficient simultaneous reconstruction technique for tomographic particle image velocimetry. *Experiments in Fluids*, 47(4-5):553–568, 2009.

[17] C Atkinson, S Coudert, J-M Foucaut, M Stanislas, and J Soria. The accuracy of tomographic particle image velocimetry for measurements of a turbulent boundary layer. *Experiments in fluids*, 50(4):1031–1056, 2011.

[18] J Belden, TT Truscott, MC Axiak, and AH Techet. Three-dimensional synthetic aperture particle image velocimetry. *Measurement Science and Technology*, 21(1):5403, December 2010.

[19] EH Adelson and JYA Wang. Single Lens Stereo with a Plenoptic Camera. *IEEE Transactions on Pattern Analysis and Machine Intelligence*, 14(2):99–106, February 1992.

[20] TW Fahringer, KP Lynch, and BS Thurow. Volumetric particle image velocimetry with a single plenoptic camera. *Measurement Science and Technology*, 26(11):115201, 2015.

[21] S Shi, J Ding, TH New, and J Soria. Light-field camera-based 3D volumetric particle image velocimetry with dense ray tracing reconstruction technique. *Experiments in Fluids*, 58(7):78, 2017.

[22] S Shi, J Ding, C Atkinson, J Soria, and TH New. A detailed comparison of single-camera light-field PIV and tomographic PIV. *Experiments in Fluids*, 59(3):1690, February 2018.

[23] T van Overbrüggen, M Klaas, J Soria, and W Schröder. Experimental analysis of particle sizes for PIV measurements. *Measurement Science and Technology*, 27(9):094009, September 2016.

[24] J Bosbach, M Kühn, and C Wagner. Large scale particle image velocimetry with helium filled soap bubbles. *Experiments in Fluids*, 46(3):539–547, 2008.

[25] N A Buchmann, C Cierpka, C J Kahler, and J Soria. Ultra-high-speed 3D astigmatic particle tracking velocimetry: application to particle-laden supersonic impinging jets. *Experiments in Fluids*, 55(11):1842.

[26] NA Buchmann, CE Willert, and J Soria. Pulsed, high-power LED illumination for tomographic particle image velocimetry. *Experiments in Fluids*, 53:1545–1560, 2012.

[27] C Willert. Stereoscopic digital particle image velocimetry for application in wind tunnel flows. *Measurement Science and Technology*, 8(12):1465–1479, 1997.

[28] B Wieneke. Stereo-PIV using self-calibration on particle images. *Experiments in Fluids*, 39(2):267–280, May 2005.

[29] B Wieneke. Volume self-calibration for 3D particle image velocimetry. *Experiments in Fluids*, 45(4):549–556, 2008.

[30] J. Soria. An investigation of the near wake of a circular cylinder using a video-based digital cross-correlation particle image velocimetry technique. *Exp. Thermal Fluid Sci.*, 12:221–233, 1996.

[31] S Shi, J Wang, J Ding, Z Zhao, and TH New. Parametric study on light field volumetric particle image velocimetry. *Flow Measurement and Instrumentation*, 49:70–88, June 2016.

[32] A Ooi, J Martin, J Soria, and MS Chong. A study of the evolution and characteristics of the invariants of the velocity gradient tensor in isotropic turbulence. *Journal of Fluid Mechanics*, 381:141–174, 1999.

[33] Joseph W Goodman. *Introduction to Fourier Optics*. McGraw-Hill, second edition edition, January 1996.

[34] L Onural and PD Scott. Digital decoding of in-line holograms. *Optical Engineering*, 26:1124–1132, November 1987.

[35] J Soria and C Atkinson. Towards 3C-3D digital holographic fluid velocity vector field measurement—tomographic digital holographic PIV (Tomo-HPIV). *Measurement Science and Technology*, 19(7):4002, July 2008.

[36] D Nguyen, D Honnery, and J Soria. Measuring evaporation of micro-fuel droplets using magnified DIH and DPIV. *Experiments in Fluids*, 50(4):949–959, April 2011.

[37] J Sheng, E Malkiel, and J Katz. Using digital holographic microscopy for simultaneous measurements of 3D near wall velocity and wall shear stress in a turbulent boundary layer. *Experiments in Fluids*, 45:1023–1035, 2008.

[38] D Schanz, S Gesemann, and A Schröder. Shake-The-Box: Lagrangian particle tracking at high particle image densities. *Experiments in Fluids*, 57(5), May 2016.